# JOURNAL PRE-PROOF

This is an early version of the article, published prior to copyediting, typesetting, and editorial correction. The manuscript has been accepted for publication and is now available online to ensure early dissemination, author visibility, and citation tracking prior to the formal issue publication.

It has not undergone final language verification, formatting, or technical editing by the journal's editorial team. Content is subject to change in the final Version of Record.

To differentiate this version, it is marked as "PRE-PROOF PUBLICATION" and should be cited with the provided DOI. A visible watermark on each page indicates its preliminary status.

The final version will appear in a regular issue of *Engineering Transactions*, with final metadata, layout, and pagination.

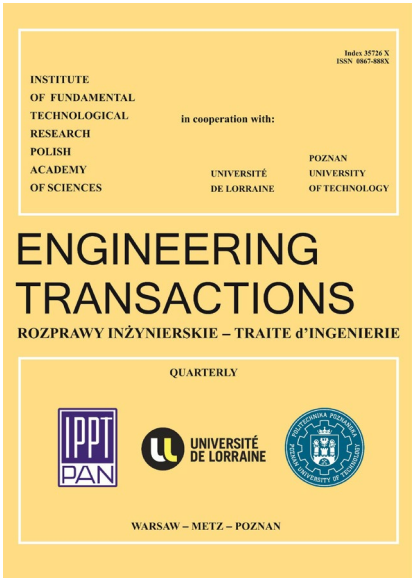


**Title:** Global buckling of a thin-walled T-frame with consideration of the shear effect

**Author(s):** Krzysztof Magnucki, Paweł Jasion

**DOI:** https://doi.org/10.24423/engtrans.2026.3641

**Journal:** *Engineering Transactions*

**ISSN:** 0867-888X, e-ISSN: 2450-8071

**Publication status:** In press

**Received:** 2025-

**Revised:** 2025-

**Accepted:** 2025-12-22

**Published pre-proof:** 2026-01-14

**Please cite this article as:**

Magnucki K., Jasion P., Global buckling of a thin-walled T-frame with consideration of the shear effect, *Engineering Transactions*, 2026, https://doi.org/10.24423/engtrans.2026.3641

Copyright © 2026 The Author(s).
This work is licensed under the Creative Commons Attribution 4.0 International CC BY 4.0.

# Global buckling of a thin-walled T-frame with consideration of the shear effect

Krzysztof MAGNUCKI[a], Paweł JASION[b*]

[a] *Łukasiewicz Research Network – Poznan Institute of Technology, 6 Ewarysta Estkowskiego St. 61-755 Poznan, Poland*

[b] *Institute of Applied Mechanics, Poznan University of Technology, ul. Jana Pawla II 24, Poznan, 61-965, Poland*

[*] *Corresponding Author e-mail: pawel.jasion@put.poznan.pl*

The work concerns the global elastic buckling problem of a thin-walled T-frame with consideration of the shear effect. A novel approach was used to account for this effect namely the non-linear shear deformation theory which gives as a result the shear deformation function describing the behaviour of the beam cross-section. This thin-walled T-frame consists of horizontal beam and vertical column made of the same standard H-beams. The shape of this standard H-beam and the dimensionless deformation function of the plane cross-section, being the result of the shear effect, are analytical described. The buckling problem of the frame is analytically formulated and solved. The critical loads of exemplary beams are analytically determined. Moreover, a numerical FEM model of the frame is elaborated and the critical loads of exemplary frames are determined. Consequently, the research results obtained by both methods are compared and the advantages of the proposed approach is discussed.

**Keywords:** elastic buckling; frame; H-beam; thin-walled beam; shear effect

## 1. Introduction

Thin-walled beams used in the 20th century are also commonly used today for example in vehicles and building steel structures. They are parts of frames containing from several to several dozen of beams. Particular beams can be subjected to different types of load like compression, twisting or bending but usually in each beam a complex state of stress is present. For this reason an effective tool is needed to analyse the state of stress in the beam, the phenomena in the junction between them but also the influence of individual beams on each other. Detailed description of the strength and stability problems of thin-walled beams and selected structures is provided by Trahair *et al.* [1]. Authors described in detail problems related to tension and compression members, local buckling of thin-plate elements, bending and lateral buckling of beams, beam-columns, frames, joints and torsion members.

The application of Generalised Beam Theory (GBT) for the analyses of thin-walled frames is presented by Basaglia *et al.* [2]. The buckling analysis of frames made of U- and I-sections is discussed including problems related to joints. These considerations are continued in the paper by Basaglia *et al.* [3]. Here the local and distortional buckling

PRE-PROOF PUBLICATION

PRE-PROOF PUBLICATION ENGINEERING TRANSACTIONS

are included. Exemplary calculations are made for L-shaped and portal frames made of open cross-section beams. The possibility of application of GBT-based finite element calculations for analysis of frames made of thin-walled members of different cross-sections is reported by Camotim *et al.* [4]. The analyses are broadened to the non-linear range and the results compared with these given by the commercial ANSYS code. The possible future development of the proposed method is discussed.

The behaviour of frames made of thin-walled members is influenced by the behaviour of its individual elements – a single beam. For this reason, an optimal shape of the cross-section is sought that will provide the highest stiffness and resistance to buckling. Examples of atypical cross-sections are shown by Magnucka-Blandzi and Magnucki [5]. Different types of channel beams are considered. Analytical formula for critical stress is obtained followed by the optimization process showing the relation between the geometrical dimensions of the cross-section and the critical stress. For selected beam experimental results are shown.

Rectangular frames are parts of vehicle structures and thus loaded with combined load, mainly by bending and torsional moments. The analytical description of global buckling of such frame made of thin-walled open cross-sections is described by Magnucki and Milecki [6]. The critical values of forces loading the frame in its plane are determined. The obtained results are compared with these from the finite element method. Stable and unstable regions for the structure are defined on plots.

Large frames in the form of spatial structures are used in construction engineering as a basis of e.g. warehouses. The behaviour of such large frames is analysed by Nagy *et al.* [7]. Three variants of frame have been modelled that is pure frame, frame with the roof made of trapezoidal skin and with the roof made of sandwich panels. Numerical analyses are performed and differences in the behaviour of these three frames are discussed. The buckling length coefficient for frames are calculated by Krystosik [8] using three different approaches. The author concluded that the recommendations of the American and European codes, due to assumed simplifications, provide inaccurate results when compared to the finite element approach. Thin-walled frames are also analysed by Zhang *et al.* [9]. A new approach is proposed in which the failure criteria is based on the sum of the structural exponential strain energy density. The buckling of frames and arches made of I cross-sections is investigated by Liu *et al.* [10]. Analytical approach based on virtual work is applied to determine the critical loads for different geometries of structures. Different formulations of joint between particular beams are considered. The effectiveness of proposed solutions is proved by comparison of the results with the finite element method.

One of the most popular shapes of the beam is an H-section since it is the most effective one when bending load is considered. The H-section beam under unequal end bending moments is investigated by Giżejowski *et al.* [11]. The influence of the slenderness of the element and moment distribution on the critical state is analysed analytically. Two examples of frames made of H-section and circular section are considered loaded with a static and dynamic load. Stability of columns and beams with H and box cross-sections are analysed by Zhou *et al.* [12]. In the paper authors propose a beam-column element with plastic hinge included giving the possibility to analyse global and local buckling. Only one element is needed to predict the load bearing capacity of columns and frames. The plane frames made of I-sections are investigated analytically by Wen *et al.* [13]. A

PRE-PROOF PUBLICATION

PRE-PROOF PUBLICATION ENGINEERING TRANSACTIONS

new comprehensive approach based of the potential energy is proposed. Different formulas are used to compare their effectiveness in determining the deformation of frames after the loss of stability. Numerical approach to the stability analysis of I-beam is presented by Yang *et al.* [14]. One dimensional finite element is proposed to solve local and global buckling problems.

A crucial meaning for the load carrying capacity of frames has the connection between particular beams-columns. Such connection in the form of K-shaped braced shear panel is investigated in the paper by Xiang *et al.* [15]. The proposed new connection system is tested in laboratory under seismic load and its possibility to dissipate the energy is analysed. Experimental tests of frames are also described by Jůza *et al.* [16]. Number of tests have been carried out for portal frames made of cold-rolled hollow sections. The influence of the material nonlinearity on the deflection of frames has been shown. The results are also compared with these from the finite element analyses.

If the frame is composed of beams the thickness of which is not small or beams are short the shear stresses play the significant role. The analysis of these stresses is especially important when multilayered beams are considered. An example of research in this area is the one by Magnucki [17]. Author compares the classical zig-zag theory with the new proposal of nonlinear shear deformation theory. It was shown that the stress distribution differs significantly for models based on both theories. The proposed approach refines the shear effect in multilayered beams. The same theory was applied to analyse the vibrations of wide-flange H-beam in the paper by Magnucki [18]. The shear coefficient is derived analytically which refines the formula for natural frequencies. It was shown that the coefficient should be taken into account for short beams and its application reduces the value of natural frequency.

In the present paper the research into the application of the nonlinear shear deformation theory described by Magnucki [17, 18] is continued. Here the theory is applied to a thin-walled T-frame, shown in Fig. 1a, made of the horizontal H-beam of the length $L_1$ and the vertical H-beam-column of the length $L_2$ stiff connected together. The joint connecting the two beams of the T-frame is shown in Fig. 1b where the dimensions of the H-section are presented that is the size of the web – $h$, and the size of the flange – $b$.

The main goal of the paper are analytical and numerical (FEM) studies of elastic global buckling problem of the T-frame under the action of force $F$ applied along the central line of the column.

## 2. Analytical model of the H-beam

The detailed cross section of the H-beam is shown in Fig. 2. The thickness of the flange equals $t_f$ and the thickness of the web $b_0$. The radius between particular parts of the cross-section is equal to $r$.

The analytical description of this cross section is formulated with consideration of the following dimensionless quantities: $\eta = y/b$ – coordinate, $\beta_0 = b_0/b$, $\chi_f = t_f/b$, $\rho = r/b$ – sizes. Thus, dimensionless widths $\bar{w}$ of successive parts:

- the first interval of the upper part $-1/2 \leq \eta \leq -(\rho + \beta_0/2)$

$$\bar{w}_1^{(up)}(\eta) = \frac{w_1^{(up)}(\eta)}{b} = 2\chi_f \tag{1}$$



PRE-PROOF PUBLICATION ENGINEERING TRANSACTIONS

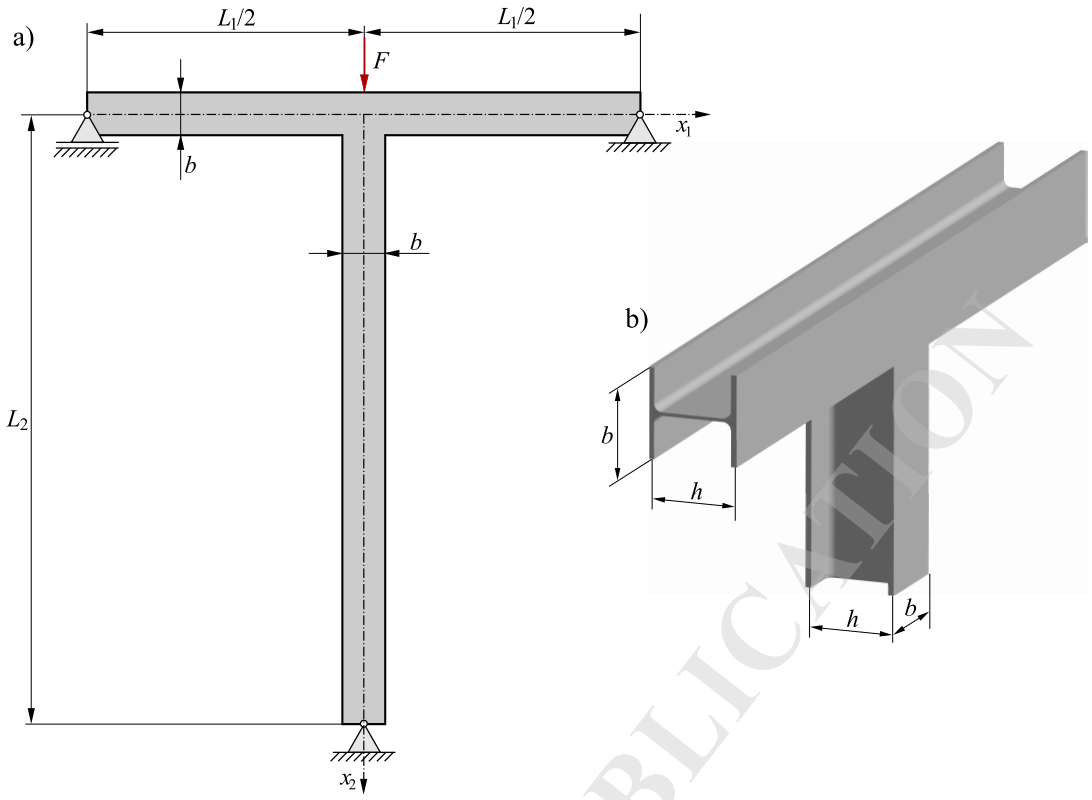


Fig. 1. Scheme of the thin-walled T-frame loaded with force $F$

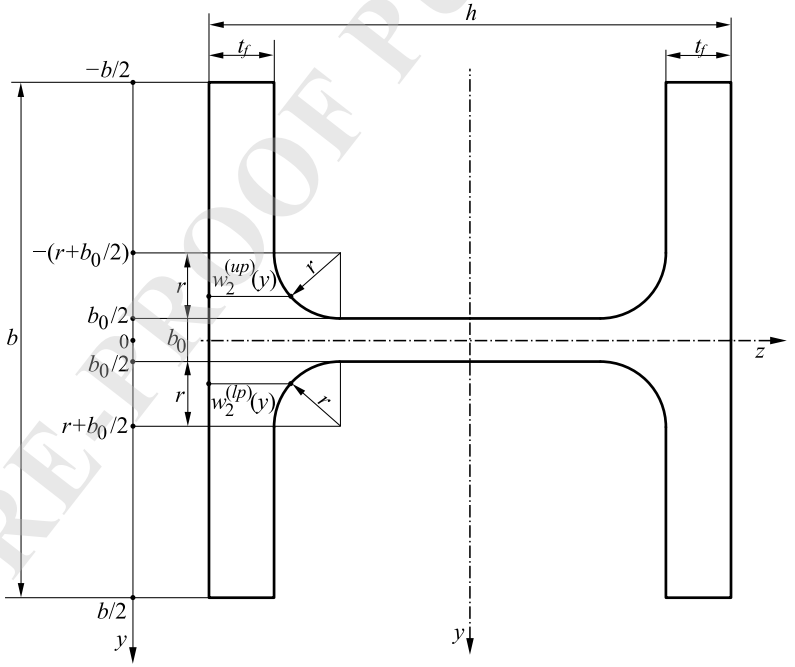


Fig. 2. Scheme of the H-beam cross section

- the second interval of the upper part $-(\rho+\beta_0/2) \le \eta \le -\beta_0/2$

$$\bar{w}_2^{(up)}(\eta) = \frac{w_2^{(up)}(\eta)}{b} = 2\left\{\chi_f + \rho - \sqrt{-\left(\eta+\frac{1}{2}\beta_0\right)\left(\eta+2\rho+\frac{1}{2}\beta_0\right)}\right\} \qquad (2)$$



PRE-PROOF PUBLICATION ENGINEERING TRANSACTIONS

- the middle part $-\beta_0/2 \leq \eta \leq \beta_0/2$

$$\bar{w}^{(mp)}(\eta) = \frac{w^{(mp)}(\eta)}{b} = \frac{h}{b} \tag{3}$$

- the second interval of the lower part $\beta_0/2 \leq \eta \leq \rho + \beta_0/2$

$$\bar{w}_2^{(lp)}(\eta) = \frac{w_2^{(lp)}(\eta)}{b} = 2\left\{\chi_f + \rho - \sqrt{\left(\eta - \frac{1}{2}\beta_0\right)\left(-\eta + 2\rho + \frac{1}{2}\beta_0\right)}\right\} \tag{4}$$

- the first interval of the lower part $\rho + \beta_0/2 \leq \eta \leq 1/2$

$$\bar{w}_1^{(lp)}(\eta) = \frac{w_1^{(lp)}(\eta)}{b} = 2\chi_f \tag{5}$$

The dimensionless widths defined above allows to calculate geometrical parameters of the cross-section that is the first moment, necessary to calculated the shears stress.

The scheme of a planar cross section deformation of this H-beam after bending-buckling is graphically presented in Fig. 3.

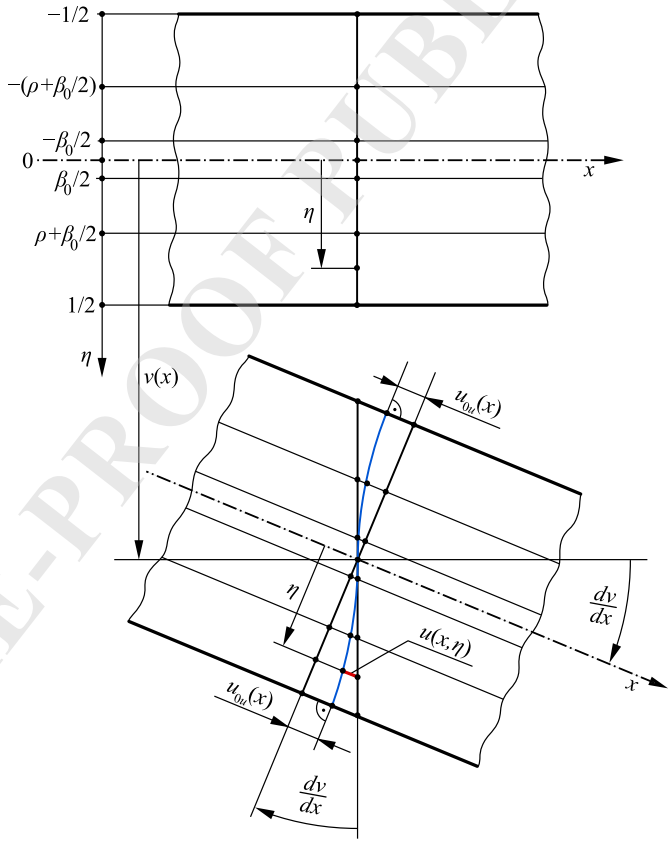


Fig. 3. Scheme of a planar cross section deformation of the H-beam

The longitudinal displacements $u$ based on the scheme (Fig. 3) and consequently normal $\varepsilon_x$ and shear $\gamma_{xy}$ strains as well as normal $\sigma_x$ and shear $\tau_{xy}$ stresses in successive parts are as follows:



PRE-PROOF PUBLICATION
PRE-PROOF PUBLICATION ENGINEERING TRANSACTIONS

- the first interval of the upper part $-1/2 \leq \eta \leq -(\rho + \beta_0/2)$

$$u_1^{(up)}(x,\eta) = -b\left[\eta\frac{dv}{dx} - f_{d1}^{(up)}(\eta)\psi(x)\right] \tag{6}$$

$$\varepsilon_{x1}^{(up)}(x,\eta) = -b\left[\eta\frac{d^2v}{dx^2} - f_{d1}^{(up)}(\eta)\frac{d\psi}{dx}\right] \tag{7}$$

$$\gamma_{xy1}^{(up)}(x,\eta) = \frac{df_{d1}^{(up)}}{d\eta}\psi(x) \tag{8}$$

$$\sigma_{x1}^{(up)}(x,\eta) = E\varepsilon_{x1}^{(up)}(x,\eta) \tag{9}$$

$$\tau_{xy1}^{(up)}(x,\eta) = \frac{E}{2(1+\nu)}\gamma_{xy1}^{(up)}(x,\eta) \tag{10}$$

- the second interval of the upper part $-(\rho + \beta_0/2) \leq \eta \leq -\beta_0/2$

$$u_2^{(up)}(x,\eta) = -b\left[\eta\frac{dv}{dx} - f_{d2}^{(up)}(\eta)\psi(x)\right] \tag{11}$$

$$\varepsilon_{x2}^{(up)}(x,\eta) = -b\left[\eta\frac{d^2v}{dx^2} - f_{d2}^{(up)}(\eta)\frac{d\psi}{dx}\right] \tag{12}$$

$$\gamma_{xy2}^{(up)}(x,\eta) = \frac{df_{d2}^{(up)}}{d\eta}\psi(x) \tag{13}$$

$$\sigma_{x2}^{(up)}(x,\eta) = E\varepsilon_{x2}^{(up)}(x,\eta) \tag{14}$$

$$\tau_{xy2}^{(up)}(x,\eta) = \frac{E}{2(1+\nu)}\gamma_{xy2}^{(up)}(x,\eta) \tag{15}$$

- the middle part $-\beta_0/2 \leq \eta \leq \beta_0/2$

$$u^{(mp)}(x,\eta) = -b\left[\eta\frac{dv}{dx} - f_{d}^{(mp)}(\eta)\psi(x)\right] \tag{16}$$

$$\varepsilon_{x}^{(mp)}(x,\eta) = -b\left[\eta\frac{d^2v}{dx^2} - f_{d}^{(mp)}(\eta)\frac{d\psi}{dx}\right] \tag{17}$$

$$\gamma_{xy}^{(mp)}(x,\eta) = \frac{df_{d}^{(mp)}}{d\eta}\psi(x) \tag{18}$$

$$\sigma_{x}^{(mp)}(x,\eta) = E\varepsilon_{x}^{(mp)}(x,\eta) \tag{19}$$

$$\tau_{xy}^{(mp)}(x,\eta) = \frac{E}{2(1+\nu)}\gamma_{xy}^{(mp)}(x,\eta) \tag{20}$$

PRE-PROOF PUBLICATION

PRE-PROOF PUBLICATION ENGINEERING TRANSACTIONS

- the second interval of the lower part $\beta_0/2 \leq \eta \leq \rho + \beta_0/2$

$$u_2^{(lp)}(x,\eta) = -b\left[\eta\frac{dv}{dx} - f_{d2}^{(lp)}(\eta)\psi(x)\right] \tag{21}$$

$$\varepsilon_{x2}^{(lp)}(x,\eta) = -b\left[\eta\frac{d^2v}{dx^2} - f_{d2}^{(lp)}(\eta)\frac{d\psi}{dx}\right] \tag{22}$$

$$\gamma_{xy2}^{(lp)}(x,\eta) = \frac{df_{d2}^{(lp)}}{d\eta}\psi(x) \tag{23}$$

$$\sigma_{x2}^{(lp)}(x,\eta) = E\varepsilon_{x2}^{(lp)}(x,\eta) \tag{24}$$

$$\tau_{xy2}^{(lp)}(x,\eta) = \frac{E}{2(1+\nu)}\gamma_{xy2}^{(lp)}(x,\eta) \tag{25}$$

- the first interval of the lower part $\rho + \beta_0/2 \leq \eta \leq 1/2$

$$u_1^{(lp)}(x,\eta) = -b\left[\eta\frac{dv}{dx} - f_{d1}^{(lp)}(\eta)\psi(x)\right] \tag{26}$$

$$\varepsilon_{x1}^{(lp)}(x,\eta) = -b\left[\eta\frac{d^2v}{dx^2} - f_{d1}^{(lp)}(\eta)\frac{d\psi}{dx}\right] \tag{27}$$

$$\gamma_{xy1}^{(lp)}(x,\eta) = \frac{df_{d1}^{(lp)}}{d\eta}\psi(x) \tag{28}$$

$$\sigma_{x1}^{(lp)}(x,\eta) = E\varepsilon_{x1}^{(lp)}(x,\eta) \tag{29}$$

$$\tau_{xy1}^{(lp)}(x,\eta) = \frac{E}{2(1+\nu)}\gamma_{xy1}^{(lp)}(x,\eta) \tag{30}$$

where $f_{d1}^{(up)}(\eta)$, $f_{d2}^{(up)}(\eta)$, $f_{d}^{(mp)}(\eta)$, $f_{d2}^{(lp)}(\eta)$, $f_{d1}^{(lp)}(\eta)$ are unknown dimensionless deformation functions, $v(x)$ is deflection function, $u_{0u}$ is the longitudinal displacement of the outside surfaces of the beam, $\psi(x) = u_{0u}/h$ is dimensionless shear effect function, $E$ is Young's modulus and $\nu$ is Poisson's ratio.

The unknown dimensionless deformation functions are analytically derived in successive parts and presented below. They are obtained by equating shear stresses formulated above with Zhuravsky's classical shear stress formula and taking into account the first moment of the cross-section of the beam. Details of this procedure can be found in papers [17] and [18]. Thus, for particular parts of the cross-section there is:

- the first interval of the upper part $-1/2 \leq \eta \leq -(\rho + \beta_0/2)$

$$f_{d1}^{(up)}(\eta) = -C_f + \frac{1}{8}\left(1 - \frac{4}{3}\eta^2\right)\eta \tag{31}$$

- the second interval of the upper part $-(\rho + \beta_0/2) \leq \eta \leq -\beta_0/2$

$$f_{d2}^{(up)}(\eta) = -C_{up} - C_{p2} + \int_{-(\rho+\beta_0/2)}^{\eta} \frac{\bar{S}_{z2}^{(up)}(\eta)}{\bar{w}_2^{(up)}(\eta)}d\eta \tag{32}$$



PRE-PROOF PUBLICATION ENGINEERING TRANSACTIONS

- the middle part $-\beta_0/2 \leq \eta \leq \beta_0/2$

$$f_d^{(mp)}(\eta) = \frac{1}{24}\left(24\frac{b}{h}C_{sz2} + 3\beta_0^2 - 4\eta^2\right)\eta \tag{33}$$

- the second interval of the lower part $\beta_0/2 \leq \eta \leq \rho + \beta_0/2$

$$f_{d2}^{(lp)}(\eta) = C_{p2} + \int_{\beta_0/2}^{\eta} \frac{\bar{S}_{z2}^{(lp)}(\eta)}{\bar{w}_2^{(lp)}(\eta)} d\eta \tag{34}$$

- the first interval of the lower part $\rho + \beta_0/2 \leq \eta \leq 1/2$

$$f_{d1}^{(lp)}(\eta) = C_f + \frac{1}{8}\left(1 - \frac{4}{3}\eta^2\right)\eta \tag{35}$$

where dimensionless coefficients:

$$C_{sz2} = \frac{1}{4}\left[1 - 4\left(\rho + \frac{1}{2}\beta_0^2\right)\right]\chi_f + \int_{-(\rho+\beta_0/2)}^{-\beta_0/2} \bar{w}_2^{up}(\eta)\eta d\eta,$$

$$C_{p2} = \frac{1}{24}\left(12\frac{b}{h}C_{sz2} + \beta_0^2\right)\beta_0, \quad C_{p1} = C_{p2} + \int_{\beta_0/2}^{\rho+\beta_0/2} \frac{\bar{S}_{z2}^{(lp)}(\eta)}{\bar{w}_2^{(lp)}(\eta)} d\eta,$$

$$C_{up} = \int_{-(\rho+\beta_0/2)}^{-\beta_0/2} \frac{\bar{S}_{z2}^{(up)}(\eta)}{\bar{w}_2^{(up)}(\eta)} d\eta, \quad C_f = C_{p1} - \frac{1}{8}\left[1 - \frac{4}{3}\left(\rho + \frac{1}{2}\beta_0\right)^2\right]\left(\rho + \frac{1}{2}\beta_0\right),$$

and dimensionless functions

$$\bar{S}_{z2}^{(up)}(\eta) = \frac{1}{4}\left[1 - 4\left(\rho + \frac{1}{2}\beta_0\right)^2\right]\chi_f + \int_{-(\rho+\beta_0/2)}^{\eta} \bar{w}_2^{(up)}(\eta)\eta d\eta,$$

$$\bar{S}_{z2}^{(lp)}(\eta) = C_{sz2} + \frac{1}{4}\left(\beta_0^2 - 4\eta^2\right)(\chi_f + \rho) + \int_{-(\rho+\beta_0/2)}^{\eta} \bar{w}_2^{(up)}(\eta)\eta d\eta.$$

These dimensionless deformation functions satisfy the continuity conditions between the successive parts of the cross section.

To solve the stability problem the principle of stationary total potential energy will be used in the form $\delta(U_{\varepsilon\gamma} - W) = 0$ (for details see [17]). The elastic strain energy $U_{\varepsilon\gamma}$ of the horizontal and vertical beam have been defined as well as the work $W$ of external load. After substituting them into the principle of stationary total potential energy and after simply transformation, the system of two differential equations of equilibrium for this H-beam is obtained in the following form:

$$\bar{J}_z \frac{d^2v}{dx^2} - C_{v\psi}\frac{d\psi}{dx} = -\frac{M_b(x)}{Eb^3h}, \tag{36}$$



PRE-PROOF PUBLICATION ENGINEERING TRANSACTIONS

$$C_{v\psi}\frac{d^3v}{dx^3} - C_{\psi\psi}\frac{d^2\psi}{dx^2} + C_{\psi}\frac{\psi(x)}{bh} = 0, \tag{37}$$

where dimensionless coefficients are as follows:

$$\bar{J}_z = \frac{1}{12}\beta_0^3 + \frac{1}{6}\left[1 - 8\left(\rho + \frac{1}{2}\beta_0\right)^3\right]\frac{b}{h}\chi_f + 2\frac{b}{h}\int\limits_{\beta_0/2}^{\rho+\beta_0/2}\eta^2\bar{w}_2^{(lp)}(\eta)d\eta,$$

$$C_{v\psi} = \int\limits_{-\beta_0/2}^{\beta_0/2}\eta f_d^{(mp)}(\eta)d\eta + 2\frac{b}{h}\left\{\int\limits_{\beta_0/2}^{\rho+\beta_0/2}\eta f_{d2}^{(lp)}(\eta)\bar{w}_2^{(lp)}(\eta)d\eta + 2\chi_f\int\limits_{\rho+\beta_0/2}^{1/2}\eta f_{d1}^{(lp)}(\eta)d\eta\right\},$$

$$C_{\psi\psi} = \int\limits_{-\beta_0/2}^{\beta_0/2}\left[f_d^{(mp)}(\eta)\right]^2 d\eta + 2\frac{b}{h}\left\{\int\limits_{\beta_0/2}^{\rho+\beta_0/2}\left[f_{d2}^{(lp)}(\eta)\right]^2\bar{w}_2^{(lp)}(\eta)d\eta + \right.$$
$$\left. + 2\chi_f\int\limits_{\rho+\beta_0/2}^{1/2}\left[f_{d1}^{(lp)}(\eta)\right]^2 d\eta\right\},$$

$$C_{\psi} = \frac{1}{2(1+\nu)}\left\{\int\limits_{-\beta_0/2}^{\beta_0/2}\left[\frac{b}{h}C_{sz2} + \frac{1}{8}\left(\beta_0^2 - 4\eta^2\right)\right]^2 d\eta + 2\frac{b}{h}\int\limits_{\beta_0/2}^{\rho+\beta_0/2}\frac{\left[\bar{S}_{z2}^{(lp)}(\eta)\right]^2}{\bar{w}_2^{(lp)}(\eta)}d\eta + \right.$$
$$\left. + \frac{\chi_f}{16}\frac{b}{h}\int\limits_{\rho+\beta_0/2}^{1/2}\left(1 - 4\eta^2\right)^2 d\eta\right\}$$

These two differential equations of equilibrium (36) and (37) are basic in the analysis of the T-frame buckling problem.

## 3. Analytical model of the thin-walled T-frame taking into account the shear effect

### 3.1. Pre-buckling state

The T-frame is statically indeterminate structure. The disconnected beams with the interaction force $F_c$ are shown in Fig. 4. The detailed scheme of the horizontal beam with the load is shown in Fig. 5. The bending moment based on this scheme is as follows

$$M_b(\xi_1) = \frac{1}{2}\xi_1\left(F - F_c\right)b\lambda_1, \tag{38}$$

where $\xi_1 = x_1/L_1$ is the dimensionless coordinate ($0 \le \xi_1 \le 1/2$) and $\lambda_1 = L_1/b$ is the relative length of the horizontal beam.

PRE-PROOF PUBLICATION

PRE-PROOF PUBLICATION ENGINEERING TRANSACTIONS

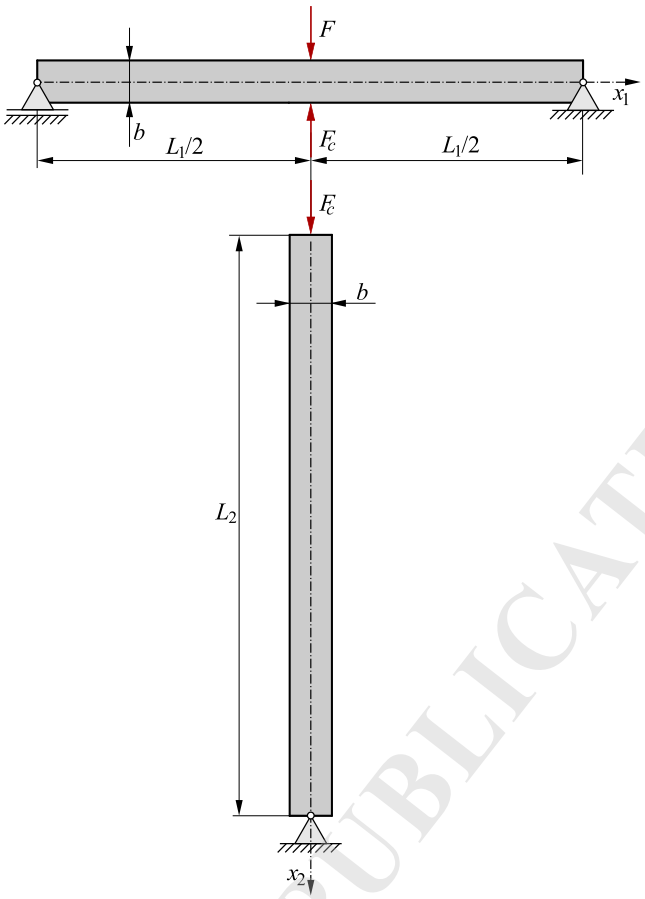


Fig. 4. Scheme of the interaction force $F_c$ of two beams

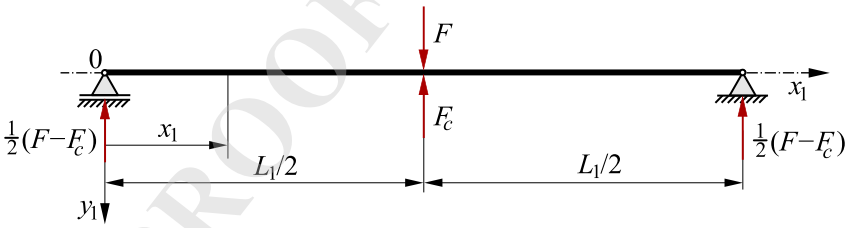


Fig. 5. Scheme of the horizontal beam with the load

Thus, the equations of equilibrium (36) and (37) in the dimensionless coordinate $\xi_1$, with consideration of the expression (38), are in the following form

$$\bar{J}_z \frac{d^2 v}{d\xi_1^2} - C_{v\psi} L_1 \frac{d\psi_{11}}{d\xi_1} = -\frac{1}{2}\xi_1 \lambda_1^3 \frac{F - F_c}{Eh}, \tag{39}$$

$$C_{v\psi} \frac{d^3 v}{d\xi_1^3} - C_{\psi\psi} L_1 \frac{d^2 \psi_{11}}{d\xi_1^2} + C_{\psi} \lambda_1^2 L_1 \frac{b}{h} \psi_{11}(\xi_1) = 0, \tag{40}$$

These equations (39) and (40), after simply transformation, are reduced to one equation in the form:

$$\frac{d^2 \psi_{11}}{d\xi_1^2} - \alpha^2 \lambda_1^2 \frac{b}{h} \psi_{11}(\xi_1) = -\frac{1}{2}\lambda_1^2 \frac{C_{v\psi}}{\bar{J}_z C_{\psi\psi} - C_{v\psi}^2} \frac{F - F_c}{Ebh} \tag{41}$$



PRE-PROOF PUBLICATION ENGINEERING TRANSACTIONS

where $\alpha = \sqrt{\dfrac{\bar{J}_z C_\psi}{\bar{J}_z C_{\psi\psi} - C_{v\psi}^2}}$ is dimensionless coefficient. The solution of this equation (41) are following functions:

$$\psi_{11}(\xi_1) = \frac{1}{2}\left\{1 - \frac{\cosh\left(\alpha\lambda_1\sqrt{b/h}\xi_1\right)}{\cosh\left(0.5\alpha\lambda_1\sqrt{b/h}\right)}\right\}\frac{C_{v\psi}}{\bar{J}_z C_\psi}\frac{F - F_c}{Eb^2} \tag{42}$$

This function satisfy the conditions: $d\psi_1/d\xi_1\big|_0 = 0$ and $\psi_1(1/2) = 0$. Substituting this function (42) into the equation (39), after integration and simply transformation, one obtains the beam deflection line

$$v(\xi_1) = \left[\left(\xi_1 - \frac{4}{3}\xi_1^3\right)\frac{b}{h} + \frac{8}{\lambda_1^2}f_{v\psi}(\xi_1)\frac{C_{v\psi}^2}{\bar{J}_z C_\psi}\right]\frac{\lambda_1^3}{16\bar{J}_z}\frac{F - F_c}{Eb} \tag{43}$$

where $f_{v\psi}(\xi_1) = \xi_1 - \dfrac{\sinh\left(\alpha\lambda_1\sqrt{b/h}\xi_1\right)}{\alpha\lambda_1\sqrt{b/h}\cosh\left(0.5\alpha\lambda_1\sqrt{b/h}\right)}$. This function (61) satisfy the conditions: $dv/d\xi_1\big|_{1/2} = 0$ and $v(0) = 0$. Thus, the maximum deflection of the horizontal beam is as follows

$$v_1 = (1 + C_{se1})\frac{\lambda_1^3}{48\bar{J}_z}\frac{F - F_c}{Eh} \tag{44}$$

where, the dimensionless shear coefficient

$$C_{se1} = \frac{12}{\lambda_1^2}\frac{h}{b}\left[1 - \frac{2}{\alpha\lambda_1}\sqrt{\frac{h}{b}}\tanh\left(\frac{1}{2}\alpha\lambda_1\sqrt{\frac{b}{h}}\right)\right]\frac{C_{v\psi}^2}{\bar{J}_z C_\psi}. \tag{45}$$

The shortening of the vertical H-beam-column under action of the force $F_c$ (Fig. 4) is as follows

$$\Delta L_2 = \frac{F_c\lambda_2}{E\bar{A}h} \tag{46}$$

where $\bar{A} = \beta_0 + 2\left\{\left[1 - 2\left(\rho + \dfrac{1}{2}\beta_0\right)\right]\chi_f + \int\limits_{\beta_0/2}^{\rho+\beta_0/2}\bar{w}_2^{(lp)}(\eta)d\eta\right\}\dfrac{b}{h}$ is the dimensionless area cross-section, $\lambda_2 = L_2/b$ is the relative length of the beam-column.

Based on the condition $v_1 = \Delta L_2$, that the deflection of the horizontal beam is consistent with the shortening of the beam-column, one obtains the force

$$F_c = \frac{(1 + C_{se1})\bar{A}\lambda_1^3}{48\bar{J}_z\lambda_2 + (1 + C_{se1})\bar{A}\lambda_1^3}F. \tag{47}$$

### 3.2. Buckling state

The form of the horizontal H-beam bending line of the T-frame after its buckling is shown in Fig. 6. The bending moment, based on this scheme, in the dimensionless coordinate $\xi_1 = x_1/L_1$ for the first interval ($0 \le \xi_1 \le 1/2$), is as follows

$$M_b(\xi_1) = -\xi_1 M_0, \tag{48}$$



PRE-PROOF PUBLICATION ENGINEERING TRANSACTIONS

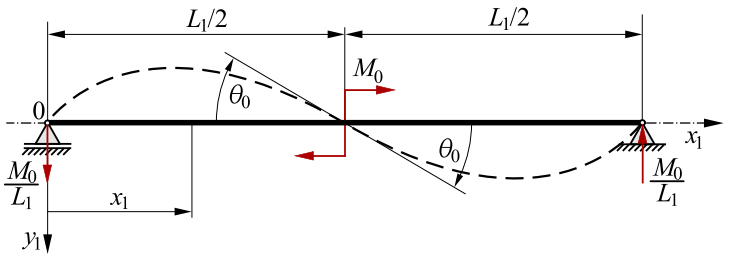


Fig. 6. Scheme of the deflection line of the horizontal H-beam

where $M_0$ is the moment of the joint connecting of two beams.

Therefore, the equation of equilibrium (36) in the dimensionless coordinate $\xi_1$, with consideration of the expression (48), is in the following form

$$\bar{J}_z \frac{d^2v}{d\xi_1^2} - C_{v\psi} L_1 \frac{d\psi_{12}}{d\xi_1} = \xi_1 \lambda_1^2 \frac{M_0}{Ebh}, \tag{49}$$

However, the equation (37) is of the form (40) with the dimensionless function $\psi_{12}(\xi_1)$. Solving these two equations (49) and (40), after simply transformation, one obtains the dimensionless function

$$\psi_{12}(\xi_1) = -\left\{1 - \frac{\cosh\left(\alpha\lambda_1\sqrt{b/h}\xi_1\right)}{\cosh\left(0.5\alpha\lambda_1\sqrt{b/h}\right)}\right\} \frac{C_{v\psi}}{\bar{J}_z C_\psi} \frac{1}{\lambda_1} \frac{M_0}{Eb^3} \tag{50}$$

and the rotation angle of the center of the deflection line

$$\theta_0 = (1 + C_{se1}) \frac{\lambda_1}{12\bar{J}_z} \frac{b}{h} \frac{M_0}{Eb^3}, \tag{51}$$

where $C_{se1}$ is the dimensionless shear coefficient consistent with the expression (45).

The buckling line form of the vertical H-beam-column is shown in Fig. 7. The bending moment, based on this scheme, in the dimensionless coordinate, is as follows

$$M_b(\xi_2) = -(1 - \xi_2)M_0 + F_c v(\xi_2), \tag{52}$$

where $\xi_2 = x_2/L_2$ is the dimensionless coordinate ($0 \le \xi_2 \le 1$), $\lambda_2 = L_2/b$ is the relative length of the vertical beam-column.

Consequently, the equations of equilibrium (36) and (37) in the dimensionless coordinate $\xi_2$, with consideration of the bending moment (52), are in the following form

$$\bar{J}_z \frac{d^2v}{d\xi_2^2} - C_{v\psi} L_2 \frac{d\psi_2}{d\xi_2} = \left[(1 - \xi_2)M_0 - F_c v(\xi_2)\right] \lambda_2^2 \frac{1}{Ebh}, \tag{53}$$

$$C_{v\psi} \frac{d^3v}{d\xi_2^3} - C_{\psi\psi} L_{12} \frac{d^2\psi_2}{d\xi_2^2} + C_\psi \lambda_2^2 L_2 \frac{b}{h} \psi_2(\xi_2) = 0. \tag{54}$$

These two differential equations, after simply transformations, are reduced to one the fourth order differential equation in the following form

$$\frac{d^4v}{d\xi_2^4} - k_1 \frac{d^2v}{d\xi_2^2} - k_2 v(\xi_2) = -(1 - \xi_2)\alpha^2 \frac{\lambda_2^4}{\bar{J}_z} \left(\frac{b}{h}\right)^2 \frac{M_0}{Eb^2}, \tag{55}$$



PRE-PROOF PUBLICATION ENGINEERING TRANSACTIONS

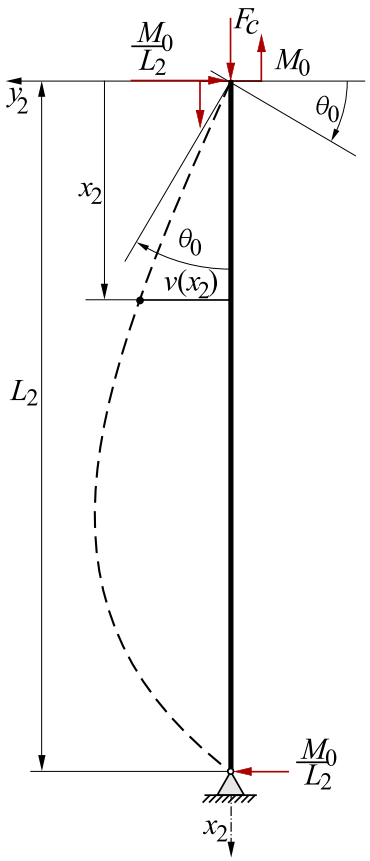


Fig. 7. Scheme buckling line form of the vertical H-beam-column

where $k_1 = \alpha^2\lambda_2^2\frac{b}{h}\left(1 - \frac{C_{v\psi}}{\bar{J}_z C_\psi}\bar{F}_c\right)$ and $k_2 = \alpha^2\frac{\lambda_2^4}{\bar{J}_z}\left(\frac{b}{h}\right)^2\bar{F}_c$ are dimensionless coefficients and $\bar{F}_c = F_c/Eb^2$ is dimensionless force.

Solving this equation, taking into account the boundary conditions $v(0) = v(1) = 0$, one obtains the buckling line of the vertical beam-column in the form

$$v(\xi_2) = \left\{1 - \xi_2 - \frac{\sin\left[(1-\xi_2)p\right]}{\sin(p)}\right\}\frac{1}{\bar{F}_c}\frac{M_0}{Eb^2} \tag{56}$$

where $p = \frac{1}{\sqrt{2}}\sqrt{-k_1 + \sqrt{k_1^2 + 4k_2}}$ is the dimensionless coefficient. Consequently, the rotation angle at the beginning of this line ($\xi_2 = 0$) is as follows

$$\theta_0 = \left.\frac{dv}{L_2 d\xi_2}\right|_0 = \left[\frac{p}{\tan(p)} - 1\right]\frac{1}{\bar{F}_c}\frac{1}{\lambda_2}\frac{M_0}{Eb^3}. \tag{57}$$

By equating rotation angles (51) and (57) one obtains the algebraic equation

$$(1 + C_{se1})\frac{\lambda_1}{12}\frac{\lambda_2}{\bar{J}_z}\frac{b}{h}\bar{F}_c + 1 - \frac{p}{\tan(p)} = 0. \tag{58}$$

Based on this equation, the dimensionless critical force $\bar{F}_{c,CR}$ for the vertical beam-column only is determined, and consequently taking into account the expression (47) one obtains

the dimensionless critical force for the whole frame

$$\bar{F}_{CR} = \left[1 + \frac{48\bar{J}_z\lambda_2}{(1+C_{se1})\bar{A}\lambda_1^3}\right]\bar{F}_{c,CR}. \tag{59}$$

# 4. Analytical model of the thin-walled T-frame neglecting shear effect

This presented frame model is a simplification of the model presented in Section 3 and is developed on the basis of the Bernoulli-Euler beam theory.

## 4.1. Pre-buckling state

The equation (39), describing the horizontal beam bending in the first interval ($0 \leq \xi_1 \leq 1/2$) (Fig. 5), without the dimensionless shear effect function $\psi_{11}(\xi_1)$, is in the following form

$$\bar{J}_z\frac{d^2v}{d\xi_1^2} = -\frac{1}{2}\xi_1\lambda_1^3\frac{F^{(o)} - F_c^{(o)}}{Eh}, \tag{60}$$

where: the superscript (o) in the forces refers to the variant without the shear effect. After integrating this equation twice and taking into account the following conditions: $v(0) = 0$ and $dv/d\xi_1|_{1/2} = 0$, one obtains the deflection line in the form

$$v\left(\xi_1\right) = \left(3 - 4\xi_1^2\right)\xi_1\frac{\lambda_1^3}{48\bar{J}_z}\frac{F^{(o)} - F_c^{(o)}}{Eh}. \tag{61}$$

Thus, the maximum deflection of this beam is as follows

$$v_1 = v\left(\frac{1}{2}\right) = \frac{\lambda_1^3}{48\bar{J}_z}\frac{F^{(o)} - F_c^{(o)}}{Eh}. \tag{62}$$

It is easy to see that this expression is the same as (44) for $C_{se1} = 0$ – omitted the shear effect.

The shortening of the vertical H-beam-column under action of the force (Fig. 5) is in the form – the expression (46). Based on the condition $v_1 = \Delta L_2$, one obtains the relationship between forces $F_c^{(o)}$ and $F^{(o)}$ in forms:

$$F_c^{(o)} = \frac{\bar{A}\lambda_1^3}{48\bar{J}_z\lambda_2 + \bar{A}\lambda_1^3}F^{(o)}, \tag{63}$$

or

$$F^{(o)} = \left(1 + \frac{48\bar{J}_z\lambda_2}{\bar{A}\lambda_1^3}\right)F_c^{(o)}. \tag{64}$$

It is easy to see that the expression (63) is the same as (47) for $C_{se1} = 0$ – omitted the shear effect.

### 4.2. Buckling state

Taking into account the Fig. 6, and the equation (49), without the dimensionless shear effect function $\psi_{12}(\xi_1)$, is in the following form

$$\bar{J}_z \frac{d^2 v}{d\xi_1^2} = \xi_1 \lambda_1^2 \frac{M_0^{(o)}}{Ebh}. \tag{65}$$

Integrating this equation twice and taking into account the conditions: $v(0) = 0$ and $v(1/2) = 0$, one obtains the horizontal beam deflection line in the form

$$v(\xi_1) = -\left(1 - 4\xi_1^2\right) \xi_1 \frac{\lambda_1^2}{24\bar{J}_z} \frac{M_0^{(o)}}{Eb^2 h}, \tag{66}$$

and consequently, the slope of this beam deflection line is as follows

$$\frac{dv}{L_1 d\xi_1} = \left(12\xi_1^2 - 1\right) \frac{\lambda_1}{24\bar{J}_z} \frac{M_0^{(o)}}{Eb^2 h}. \tag{67}$$

Thus, the rotation angle of the center of the deflection line is as follows

$$\theta_0 = \left.\frac{dv}{L_1 d\xi_1}\right|_{1/2} = \frac{\lambda_1}{12\bar{J}_z} \frac{1}{h} \bar{M}_0^{(o)}, \tag{68}$$

where $\bar{M}_0^{(o)} = M_0^{(o)}/Eb^2$ is dimensionless moment. It is easy to see that this expression is the same as (51) for $C_{se1} = 0$ – omitted the shear effect.

Taking into account the Fig. 7, and the equation (53), without the dimensionless shear effect function $\psi_2(\xi_2)$, after simply transformation is in the following form

$$\frac{d^2 v}{d\xi_2^2} + \frac{\lambda_2^2}{\bar{J}_z} \frac{b}{h} \bar{F}_c^{(o)} v(\xi_2) = (1 - \xi_2) \frac{\lambda_2^2}{\bar{J}_z} \frac{b}{h} \bar{M}_0^{(o)}, \tag{69}$$

where $\bar{F}_c^{(o)} = F_c^{(o)}/Eb^2$ is dimensionless force. Solving this second order differential equation, taking into account two boundary conditions $v(0) = v(1) = 0$, after simply transformation, one obtains the buckling line of the vertical beam-column in the form

$$v(\xi_2) = \left\{ 1 - \xi_2 - \frac{\sin\left[(1 - \xi_2) p^{(o)}\right]}{\sin\left(p^{(o)}\right)} \right\} \frac{\bar{M}_0^{(o)}}{\bar{F}_c^{(o)}}, \tag{70}$$

where $p^{(o)} = \lambda_2 \sqrt{\frac{b}{h} \frac{\bar{F}_c^{(o)}}{\bar{J}_z}}$ is dimensionless coefficient.

The slope of this buckling line is as follows

$$\frac{dv}{L_2 d\xi_2} = \left\{ -1 + f_{CR} \frac{\cos\left[(1 - \xi_2) p^{(o)}\right]}{\sin\left(p^{(o)}\right)} \right\} \frac{\bar{M}_0^{(o)}}{L_2 \bar{F}_c^{(o)}}. \tag{71}$$

Thus, the rotation angle at the beginning of this buckling line is as follows

$$\theta_0 = \left.\frac{dv}{L_2 d\xi_1}\right|_0 = \left[\frac{p^{(o)}}{\tan\left(p^{(o)}\right)} - 1\right] \frac{\bar{M}_0^{(o)}}{L_2 \bar{F}_c^{(o)}}. \tag{72}$$

By equating rotations angles (68) and (72) one obtains the algebraic equation

$$\frac{\lambda_1\lambda_2}{12\bar{J}_z}\frac{b}{h}\bar{F}^{(o)}_{c,CR} + 1 - \frac{p^{(o)}}{\tan\left(p^{(o)}\right)} = 0. \tag{73}$$

Based on this equation, the dimensionless critical force $F^{(o)}_{c,CR}$ for the vertical beam-column is determined, and in accordance with the expression (64) one obtains the dimensionless critical force for the T-frame without shear effect

$$\bar{F}^{(o)}_{CR} = \left(1 + \frac{48\bar{J}_z\lambda_2}{\bar{A}\lambda_1^3}\right)\bar{F}^{(o)}_{c,CR}. \tag{74}$$

It is easy to see that this expression is the same as (59) for $C_{se1} = 0$ – omitted the shear effect.

## 5. Analytical studies of selected T-frames

Example analytical studies are carried out for thin-walled T-frame made of the horizontal beam of relative lengths $\lambda_1 = 10, 15, 20, 30, 40$ and the vertical beam-column of relative length $\lambda_2 = 40$. Sizes of three standard H-beams are shown in Table 1.

Table 1. Sizes of three selected standard H-beams

| Sizes | $h$ [mm] | $b$ [mm] | $b_0$ [mm] | $t_f$ [mm] | $r$ [mm] |
|---|---|---|---|---|---|
| H-300 | 300 | 300 | 11.0 | 19.0 | 27.0 |
| H-400 | 400 | 300 | 13.5 | 24.0 | 27.0 |
| H-500 | 500 | 300 | 14.5 | 28.0 | 27.0 |

Values of dimensionless critical forces calculated on the basis of the equation (58) and the expression (59) for the case of shear effect taking into accound and equation (73) and expression (74) neglecting this effect are presented in Tables 2, 3 and 4.

Table 2. Critical forces of T-frame made of standard H-300 beams

| $\lambda_1$ | 10 | 15 | 20 | 30 | 40 |
|---|---|---|---|---|---|
| $10^4\bar{F}_{c,CR}$ | 1.24240 | 1.22063 | 1.19980 | 1.16123 | 1.12664 |
| $10^4\bar{F}^{(o)}_{c,CR}$ | 1.28132 | 1.25771 | 1.23422 | 1.19230 | 1.15505 |
| $10^4\bar{F}_{CR}$ | 1.39063 | 1.26442 | 1.21805 | 1.16648 | 1.12880 |
| $10^4\bar{F}^{(o)}_{CR}$ | 1.43833 | 1.30273 | 1.25312 | 1.19771 | 1.15726 |

By comparing the values of critical forces determined analytically with and without taking into account the shear effect, it is easy to see that the shear effect reduces the values of critical forces. Differences between these values of critical forces are specified in Table 5.

Moreover, these results of the exemplary calculations are graphically presented in the next section and compared with the results of FE analyses.

Table 3. Critical forces of T-frame made of standard H-400 beams

| $\lambda_1$ | 10 | 15 | 20 | 30 | 40 |
|---|---|---|---|---|---|
| $10^4\bar{F}_{c,CR}$ | 1.55404 | 1.52748 | 1.50195 | 1.45453 | 1.41189 |
| $10^4\bar{F}^{(o)}_{c,CR}$ | 1.61894 | 1.58832 | 1.55942 | 1.50646 | 1.45940 |
| $10^4\bar{F}_{CR}$ | 1.72912 | 1.57947 | 1.52337 | 1.46080 | 1.41446 |
| $10^4\bar{F}^{(o)}_{CR}$ | 1.80787 | 1.64324 | 1.58217 | 1.51297 | 1.46206 |

Table 4. Critical forces of T-frame made of standard H-500 beams

| $\lambda_1$ | 10 | 15 | 20 | 30 | 40 |
|---|---|---|---|---|---|
| $10^4\bar{F}_{c,CR}$ | 1.79638 | 1.76636 | 1.73741 | 1.68347 | 1.63484 |
| $10^4\bar{F}^{(o)}_{c,CR}$ | 1.88901 | 1.85329 | 1.81957 | 1.75777 | 1.70286 |
| $10^4\bar{F}_{CR}$ | 1.99066 | 1.82430 | 1.76165 | 1.69048 | 1.63777 |
| $10^4\bar{F}^{(o)}_{CR}$ | 2.10220 | 1.91526 | 1.84523 | 1.76512 | 1.70586 |

Table 5. Differences between the values of critical forces with and without the shear effect

| $\lambda_1$ | 10 | 15 | 20 | 30 | 40 |
|---|---|---|---|---|---|
| $\Delta\bar{F}^{(H-300)}_{CR}\%$ | 3.4 | 3.0 | 2.9 | 2.7 | 2.5 |
| $\Delta\bar{F}^{(H-400)}_{CR}\%$ | 4.6 | 4.0 | 3.9 | 3.6 | 3.4 |
| $\Delta\bar{F}^{(H-500)}_{CR}\%$ | 5.6 | 5.0 | 4.7 | 4.4 | 4.2 |

## 6. Numerical (FEM) studies of selected T-frames

As a comparative study a finite element analysis has been performed. A 3D model of the whole frame has been prepared. A linear buckling analysis has been made using the Ansys software [19]. The material's model has been assumed to be a linear elastic with the following parameters: Young modulus $E = 200000$ MPa and Poisson ratio $\nu = 0.3$. The boundary conditions applied to the model are shown in Fig. 8a. All three ends of the frame are pin-supported. A remote displacement option was used to achieve this condition that was applied to the whole cross-section and realised at its centroid. At the bottom of the vertical part of the frame displacements along three axes are blocked. The rotation around the axis $z$ is allowed. Both ends of the horizontal part can move horizontally and rotate around the $z$ axis. To avoid a rigid body motion the horizontal displacement has been taken away at one node in the mid-length of the horizontal beam. The force $F$ has been applied to the upper part of this beam at the edge corresponding to the center line of the web of the vertical part of the frame (see Fig. 8a).

To discretize the model of the frame solid elements have been used marked as *solid186* which were tetrahedral, second order finite elements with 10 nodes and 3 degrees of freedom in each node – displacements according three axes. This choice provides the

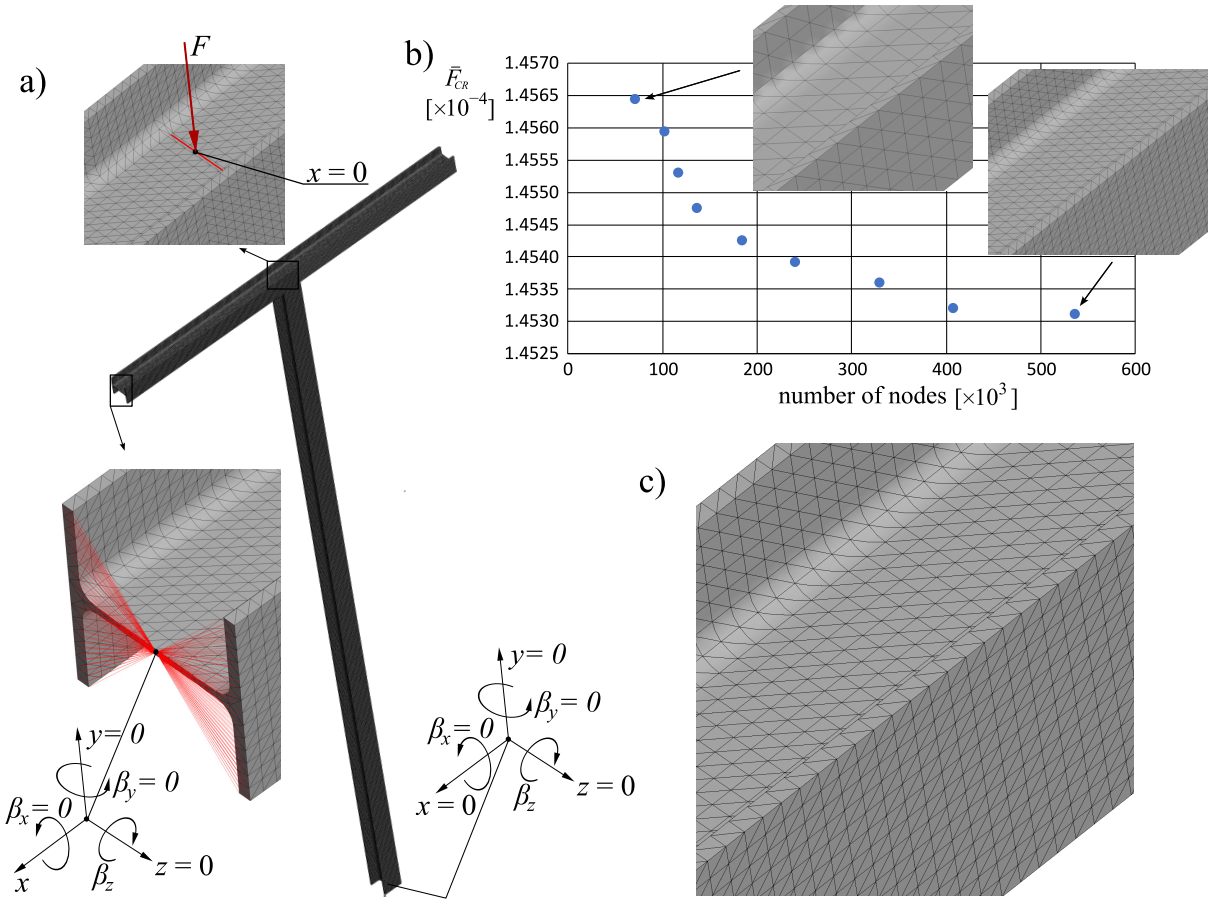


Fig. 8. FE model of the T-frame: a) boundary conditions; b) mesh convergency study; c) mesh pattern

most effective model among others investigated in which both tetrahedral and hexahedral elements were taken into account. The negative influence of using a single element over the thickness of the beam wall was also verified. The number of elements has been established based on the mesh convergency analysis presented in Fig. 8b. It was decided to set the element size to 22 which gave about 400000 nodes for the frame H-300 with the parameter $\lambda_1 = 10$. It should be noted that even for the two extreme cases considered, shown in Fig. 8b, the difference in value of buckling load is only about 0.2%. It comes from the fact that the buckling mode has a global character and the analysis is a linear one. The exemplary mesh used in all analyses is shown in Fig. 8c.

Typical buckling shapes corresponding to frame H-300 are shown in Fig. 9 for selected lengths of the horizontal beam. The values of the buckling load for all considered frames are presented on plots in Fig. 10 together with the results given by the analytical solution described in the previous section. They are given on the vertical axis whereas the horizontal axis corresponds to the length parameter $\lambda_1$ – the higher its value the longer the horizontal part of the frame. As to the analytical solution two curves are shown. One of them corresponds to the buckling load for the whole frame – red line with circles, and the second one corresponds to the buckling of the vertical beam only – blue line with diamonds. In FE analysis only the whole frame was analysed and its results are marked with black crosses.

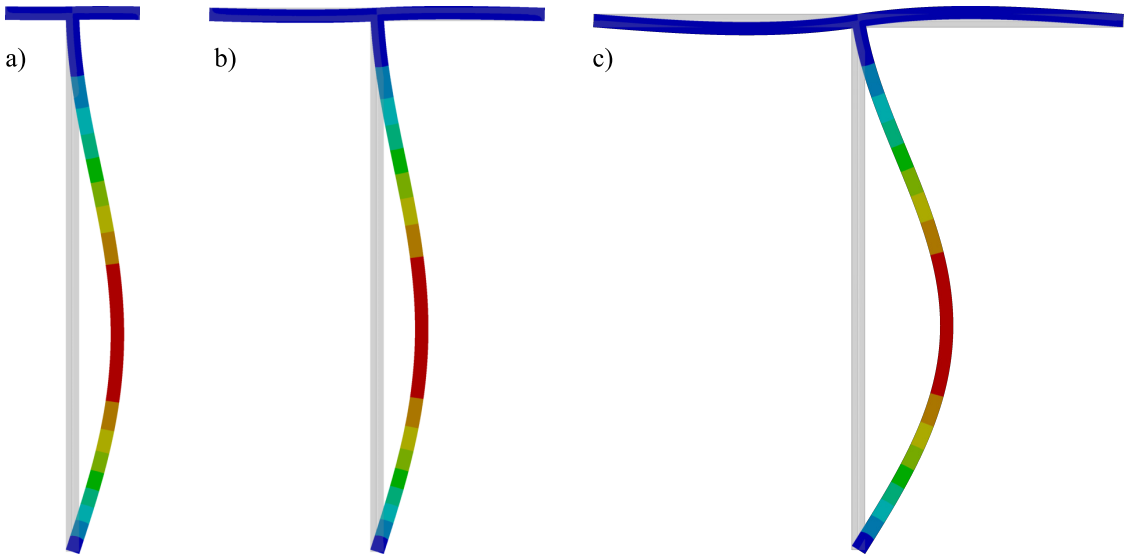


Fig. 9. First buckling mode of T-frame H-300 for different $\lambda_1$: a) $\lambda_1 = 10$; b) $\lambda_1 = 25$; c) $\lambda_1 = 40$ (scaled $10^3$)

## 7. Discussion of the results

The results presented above have been obtained with the use of the analytical model and with the use of the numerical approach. In both ways linear behaviour of the material has been assumed. In analytical model the shearing stresses were taking into account.

For all considered examples the shape of the frame after the loss of stability was the same and consistent with these shown in Fig. 9 on which the presented deformation is magnified $10^3$ times for better visualisation. The vertical part buckles like the column hinged supported at the bottom and hinged or stiff supported at the top. The latter depends on the length of the horizontal beam. If the beam is short it works similar to fixed support and the rotation at this point is small. The longer the beam the smallest its influence on the behaviour of the column which will deform as hinged supported at both ends if the beam is long enough. This relation is also visible in the values of the buckling loads obtained from the analytical solution. The longer the horizontal beam is the closer the value of the buckling load of the frame is (red line in Fig. 10) to the value corresponding to the case when only column is considered (blue line). In presented examples for $\lambda_1 = 40$ the buckling load for the frame is only 0.2% higher than this for the column. This means that the influence of the horizontal beam on the stability of the whole structure is negligible.

The distribution of the results given by the FE analyses (black crosses in Fig. 10) is similar to these from analytical solution. They are slightly above the red curve. The smallest difference was noted for the frame H-300 with $\lambda_1 = 40$ and equal to 3% and the biggest difference, 6%, for the frame H-500 with $\lambda_1 = 10$. However, the FE results are very close to the analytical solution in which shear effect is omitted (green line – B-E) – the discrepancy does not exceed 1%. Since the influence of the finite element type on the results has been eliminated and a number of boundary conditions has been verified, the agreement between the FE results and the B-E theory may be the result of the linear nature of the buckling analysis, which is not able to capture the shear effect phenomenon.

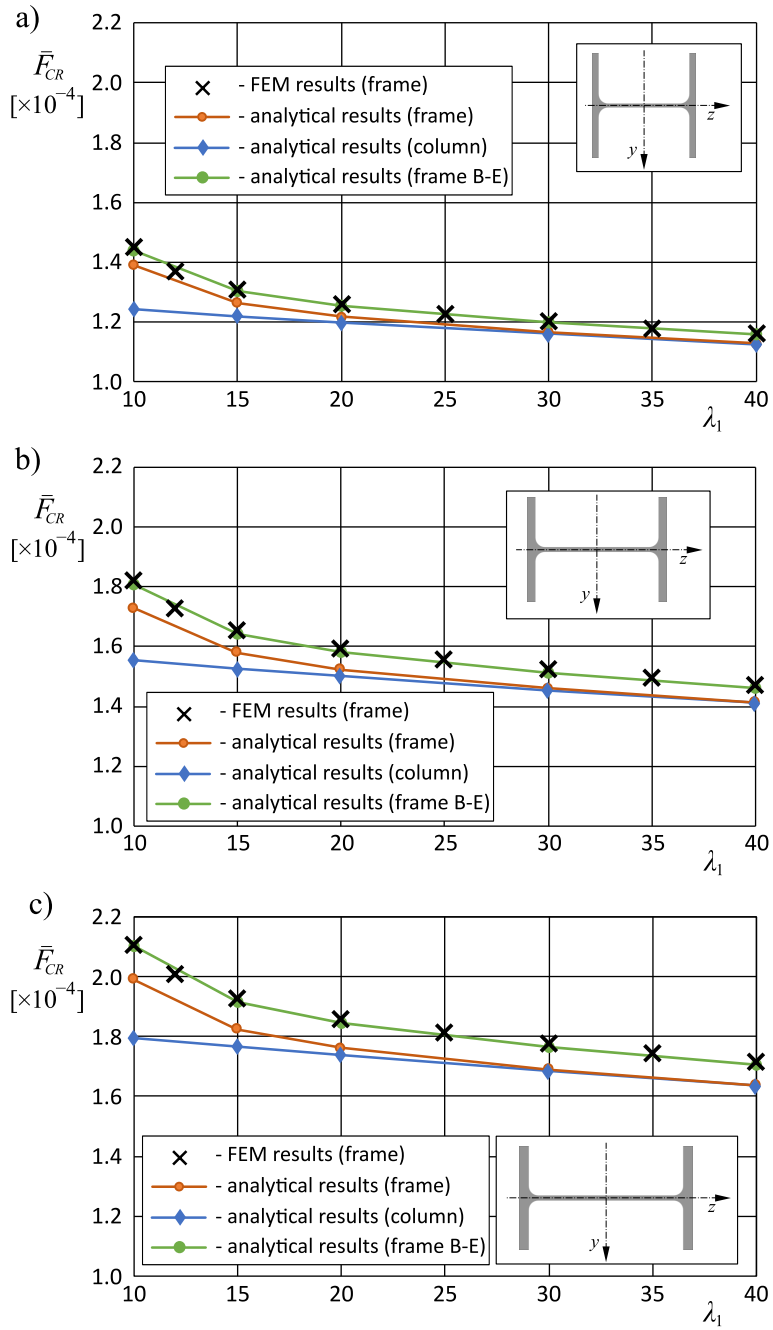


Fig. 10. Comparison of dimensionless buckling loads obtained with analytical and numerical approach: a) H-300; b) H-400; c) H-500

## 8. Conclusions

In the present work the problem of stability of the T-frame has been solved analytically and numerically. The novelty of the analytical approach proposed in the paper lies in the fact that the influence of the shear stress on the deformation of the frame is taken into account at the model definition. This makes analytical calculations more realistic especially when short beams are considered and at the same time makes the structure safer. The defined shear coefficient allows to determine the contribution of the shear

stress to the critical load. Presented formulae gives more conservative results even when compared to the numerical calculations since inclusion the shear effect reduces the stiffness of the structure and thus lowers the value of the buckling load. The obtained buckling loads are consistent for both approaches and the biggest difference between the analytical and numerical solution equals 6%. Additional FE analyses have to be performed regarding the compatibility of both methods with emphasis on FE modelling details like the type and number of elements or the way of load and support.

The presented approach has a general form and can be applied to different shapes of the cross-section. Further broad investigation, including experimental tests, might validate its correctness and explain the influence of the shearing stress on the behaviour of engineering structures.

## Acknowledgements

The paper is developed based on the scientific activity of the Łukasiewicz Research Network – Poznan Institute of Technology and the statutory activity of the Poznan University of Technology (Grant of the Ministry of Science and Higher Education in Poland no 0612/SBAD/3628).

## Declaration of Conflicting Interest

The Authors declare that there are no known competing financial interests or personal relationships that could influence the work reported in this paper.

## References

[1] Trahair N.S., Bradford M.A., Nethercot D.A., Gardner L., *The Behaviour and Design of Steel Structures to EC3*, 4 ed., Taylor & Francis Group, London 2008.

[2] Basaglia C., Camotim D., Silvestre N., Global buckling analysis of plane and space thin-walled frames in the context of GBT, *Thin-Walled Structures*, **46**(1):79–101, 2008, doi:10.1016/j.tws.2007.07.007.

[3] Basaglia C., Camotim D., Silvestre N., GBT-based local, distortional and global buckling analysis of thin-walled steel frames, *Thin-Walled Structures*, **47**(11):1246–1264, 2009, doi:10.1016/j.tws.2009.04.003.

[4] Camotim D., Basaglia C., Silvestre N., GBT buckling analysis of thin-walled steel frames: A state-of-the-art report, *Thin-Walled Structures*, **48**(10–11):726–743, 2010, doi:10.1016/j.tws.2009.12.003.

[5] Magnucka-Blandzi E., Magnucki K., Buckling and optimal design of cold-formed thin-walled beams: Review of selected problems, *Thin-Walled Structures*, **49**(5):554–561, 2011, doi:10.1016/j.tws.2010.09.011.

[6] Magnucki K., Milecki S., Elastic buckling of a thin-walled rectangular frame under in-plane compression, *Thin-Walled Structures*, **116**:326–332, 2017, doi:10.1016/j.tws.2017.03.007.

[7] Nagy Z., Kelemen A., Nedelcu M., The influence on portal frame buckling of different cladding systems – a comparative numerical study considering stressed skin effect, *Thin-Walled Structures*, **182**:110310, 2023, doi:10.1016/j.tws.2022.110310.

[8] Krystosik P., On the columns buckling length of unbraced steel frames with semi-rigid joints, *Archives of Civil Engineering*, **67**(1):539–556, 2021, doi:10.24425/ace.2021.136488.

[9] Zhang M., Xie X., Gao X., Pan Y., Parke G., Study on failure criterion of thin-walled steel frame structures based on the esed parameter, *Thin-Walled Structures*, **161**:107357, 2021, doi:10.1016/j.tws.2020.107357.

[10] Liu Y., Yang Y., Liu X., Guo D., Lateral-distortional buckling of frames composed of non-aligned i-members by a simple distortional beam element considering angling effect, *Thin-Walled Structures*, **202**:112146, 2024, doi:10.1016/j.tws.2024.112146.

[11] Giżejowski M., Szczerba R., Stachura Z., Gajewski M., Buckling resistance of quasi-straight h-section beam-columns under unequal end moments, *Archives of Civil Engineering*, **67**(1):323–349, 2021, doi:10.24425/ace.2021.136476.

[12] Zhou Y., Ning S., Huang D., Li Y., Refined plastic hinge method for steel frames with local–global interactive buckling, *Thin-Walled Structures*, **181**:110013, 2022, doi:10.1016/j.tws.2022.110013.

[13] Wen Y., He W., Zhan W., Li B., Full beam formulation for the lateral torsional buckling analysis of elastic frames by considering the structural detail of beam-to-column joint, *Thin-Walled Structures*, **183**:110414, 2023, doi:10.1016/j.tws.2022.110414.

[14] Yang Y., Hui Y., Li P., Yang Y., Huang Q., Giunta G., Belouettar S., Hu H., Global/local buckling analysis of thin-walled I-section beams via hierarchical one-dimensional finite elements, *Engineering Structures*, **280**:115705, 2023, doi:10.1016/j.engstruct.2023.115705.

[15] Xiang Y., Zhou X., Shi Y., Zhou J., Ke K., Deng F., Study on the seismic performance of cold-formed thin-walled steel frame with K-shaped braced shear panel, *Thin-Walled Structures* **184**:110449, 2023, doi:10.1016/j.tws.2022.110449.

[16] Jůza J., Jandera M., Křemen T., Experimental investigation on the square and rectangular hollow section stainless steel portal frames, *Thin-Walled Structures*, **189**:110897, 2023, doi:10.1016/j.tws.2023.110897.

[17] Magnucki K., Bending of a five-layered composite beam with consideration of two analytical models, *Archive of Mechanical Engineering* **71**(1):27–46, 2024, doi:10.24425/ame.2024.149188.

[18] Magnucki K., Free flexural vibrations of standard wide-flange H-beams with consideration of the shear effect, *Rail Vehicles/Pojazdy Szyn.*, (1-2):46–50, 2024, doi:10.53502/RAIL-189244.

[19] Ansys®, Academic Research Mechanical Release 2023 R2, Ansys, Inc., 2023.